Improvement in Carrier Mobility of ZnON Transistor by Tantalum Encapsulation

Min Jae Kim[1], Jae Kyeong Jeong[1]

[1]Hanyang University

Keywords: Thin-film Transistors, Zinc oxynitride, Tantalum oxide, Scavenging effect, Encapsulation

ABSTRACT

The TaOx/ZnON thin-film stack showed a more uniform distribution of nanocrystalline ZnON with an increased stoichiometric anion lattice compared to control ZnON thin-films. Significantly, improved mobility of 89.4 cm2/Vs were achieved for TaOx/ZnON TFTs. This improvement can be explained by the removal and passivation effect of TaOx film on ZnON..

1 INTRODUCTION

Recently, due to low electron effective mass and high carrier mobility, zinc oxynitride (ZnON) materials were proposed as a promising n-type semiconductor. [1-3] Optical band-gap (E_g), effective carrier mobility, and density of the ZnON thin films can be controlled by the ratio of anions of wurtzite ZnO (E_g ~3.2 eV) and cubic Zn_3N_2 (E_g ~1.0 eV).[2] As nitrogen enters the oxygen sites in ZnON, the nitrogen 2p band overlaps with the oxygen 2p band, which narrows the bandgap.[2] Thus, in ZnON, neutral V_O defects near the VB edge could be covered, which strengthen the persistent photoconductivity (PPC) effect and negative bias illumination stress (NBIS)-induced V_{TH} instability resistance in ZnO and AOS TFTs.[2,4,5]

Due to these several benefits, the effects of annealing temperature and composition ratio on electrical properties of ZnON thin films have been intensively studied.[6-8] Although these merits, the chemical instability of ZnON materials is difficult to apply commercially. Because Zn-N chemical bonds are weak, nitrogen-related defects and out-diffusion cause electrical properties and long-term deterioration.[9]

In this paper, a scavenge effect induced by tantalum oxide film was investigated to improve the chemical and electrical stabilities of ZnON TFTs. These TFTs fabricated with this encapsulation and achieved a high field-effect mobility of 89.4 cm^2/Vs, low subthreshold gate swing of 0.33 V/decade, high $I_{ON/OFF}$ ratio of 8.6 * 10^8, and long-term storage stability.

2 EXPERIMENT

ZnON TFTs with an inverted staggered bottom-gate and top-contact structure were fabricated on Si substrates. A 100 nm-thick SiO_2 gate insulator layer was grown via thermal oxidation onto a heavily-doped p-type Si wafer. The heavily-doped Si substrate acted as the gate electrode. A 20 nm-thick ZnON channel layer was deposited via a reactive sputtering process where the $Ar/O_2/N_2$ reactive gas ratio, DC power, and chamber pressure during channel preparation were 5/2.5/30, 100 W, and 5 mTorr, respectively. An ITO film was used as the source/drain (S/D) electrode and was deposited onto the $ZnON/SiO_2/Si$ substrate via magnetron sputtering. The DC power and chamber pressure under an Ar atmosphere were 50 W and 5 mTorr, respectively. The ZnON channel island and ITO S/D electrode were patterned through a shadow mask during sputter deposition. The width (W) and length (L) values of the ZnON TFTs were 1000 μm and 300 μm, respectively. The devices were then contact-annealed in an electric furnace for 1 h at 250 °C under an air atmosphere (hereafter referred to as the control device). A 10 nm-thick Ta film was selectively deposited via DC sputtering through a shadow mask onto the ZnON film between the source and drain electrode with dimensions of W/L = 2300 μm / 150 μm. A final post-deposition annealing (PDA) step was performed at 200 °C for 1 hour under O_2 ambient, which will be referred to as Ta-capped ZnON TFTs.

3 RESULTS & DISCUSSION

Figure 1 shows HRTEM images of the control and Ta-capped ZnON samples annealed at 200 °C for 1 hour under O^2 ambient. The periodic lattice image in Figure 1a clearly indicates that the control ZnON film is in the crystalline phase. Evolution of the selective area diffraction patterns (SADPs) yielded variations with regard to the degree of crystallization along the depth direction of the control ZnON films. ZnON films near the SiO2/Si substrate exhibited rather diffused hallow SADPs, suggesting a lack of highly ordered cations and anions. However, the SADPs of the ZnON films exhibited discernible Bragg spots with the growing direction, indicating that crystalline quality improved with an increase in deposition time. Interestingly, the depth-dependent evolution of SADPs disappeared for Ta-capped ZnON films as can be seen in Figure 1b. The Ta-

capped ZnON films exhibited better uniformity in terms of the degree of crystallization along the depth direction compared to the control ZnON films. The SADPs were identified as (400), (222), and (044) reflections of crystalline Zn_3N_2 with an anti-bixbyite structure, corresponding to an inter-planar spacing of 2.42 Å, 2.79 Å, and 1.71 Å, respectively. These values were smaller than those of conventional cubic Zn_3N_2 crystals by about 0.1% because Zn-N possesses a larger bond length than Zn-O under an identical coordination number of six (bond lengths of Zn-N and Zn-O were 2.11 Å and 1.91 Å, respectively). Therefore, the Ta-capped ZnON film can be regarded as an aggregate of O-substituted Zn_3N_2 nanocrystallites. In our previous research, a chemical reaction with a transition Ta layer enabled low-temperature crystallization of the amorphous IGZO film. The reduction in onset crystallization temperature of IGZO from > 600 °C (without catalytic layer) to 300 °C was attributed to the donation of electrons from Ta into IGZO and subsequent facile rearrangement due to the change in the bonding characteristics of the IGZO.[10] Similar Ta-induced crystallization can also occur in ZnON system. Indeed, the metallic Zn and V_O was found to exist near the TaOx/ZnON interface after 2nd PDA at 200 °C, indicating that the Zn-O bond is dissociated by the oxidation of Ta layer during PDA step. Once the nuclei were formed near the TaOx/ZnON interface, the crystalline region grew and propagated in the depth direction. It constitutes the reason for the better uniformity and crystallinity of Ta-capped ZnON compared to the control ZnON films.

Figure 2a, b shows the N 1s XP spectra of the control and Ta-capped ZnON films. Photoelectron binding energies were calibrated to the C 1s peak for C-C bonds at 284.5 eV. The N 1s peak was deconvoluted into three peaks at 395.2, 396.0, and 397.4 eV. The N 1s peaks centered at 395.2 and 396.0 were assigned to the Zn-N bonding energies for stoichiometric Zn_3N_2 and non-stoichiometric Zn_xN_y, respectively. The peak at 397.4 eV originated from N-N chemical bonds.[3-11] The increase (decrease) in intensity of stoichiometric Zn_3N_2 (non-stoichiometric Zn_xN_y) for the Ta-capped ZnON films suggested that the electrical transport properties could be substantially improved for transistors with this channel layer because point defects such as V_N in non-stoichiometric Zn_xN_y could act as potential electron trapping centers and disconnect an electron conduction pathway.[2] The O 1s XPS spectra for both ZnON films were also compared and depicted in Figure 2c, d. The asymmetric O 1s peaks were deconvoluted into three bases centered at 530.5, 531.8, and 532.8 eV. The peaks could be attributed to oxygen bonded to fully coordinated Zn ions (Zn-O lattice), under-coordinated Zn ions (oxygen vacancy, V_O), and impurity related oxygen such as hydroxyl groups (OH), respectively.[12] Compared to the control ZnON film, Ta-capped ZnON films exhibited less OH fractions as summarized in Table 1. It was noted that oxygen substituted at nitrogen sites of stoichiometric Zn_3N_2 was a shallow electron donor.[13] Thus, the free electron density (N_e) for the Ta-capped ZnO film was expected to be higher than that of the control ZnON film. It was obvious that the metal capping and subsequent annealing process was an effective method to reduce anion-related defect centers such as V_N as well as OH-related impurities within the ZnON films.

In Figure 3, The control ZnON TFT yielded a high mobility (μ_{FE}) of 36.2 cm^2/Vs, a subthreshold gate swing (SS) of 0.28 V/decade, a threshold voltage (V_{TH}) of 1.28V, and an $I_{ON/OFF}$ ratio of 2.9×10^8. The mobility for the control ZnON device with oxygen-rich anions was comparable to that for state-of-the-art ZnON TFTs reported in the literature, which can be related to the low electron effective mass of the ZnON system. By contrast, a significant performance enhancement was observed for the Ta-capped ZnON TFTs. The μ_{FE} of ~89.4 cm^2/Vs, SS of 0.33 V/decade, V_{TH} of -0.45V, and $I_{ON/OFF}$ ratio of 8.6×10^8, respectively, as summarized in Table 2. Improvements in the transport and I_{DS} modulation capability of the Ta capped ZnON TFTs were reflected in their superior output characteristics in Figures 3c, d. It was interesting to discuss the physical rationale with regard to the beneficial effects of TaO_x encapsulation in terms of mobility enhancement. Given a thermal annealing condition of 250 °C, the Gibbs free energies of formation (ΔG_f) for ZnO and Ta_2O_5 were -348.1 and -1911.2 kJ/mole, respectively. Thus, PDA of the Ta/ZnON stack at high temperature would cause oxidation of the Ta film and simultaneous reduction of the ZnON film to metallic Zn. However, if the PDA temperature was moderate (< 250 °C), the high activation energy barrier (> 1 eV) against the dissociation of Zn-O bonds would prevent strong oxidation of the TaO_x film involving the conversion of ZnON to a metallic Zn film. Instead, weakly bonded oxygen and/or nitrogen species such as OH and N-N bonds could be selectively eliminated near the back surface of the ZnON films.[1] Because those defects acted as scattering centers in ZnON, reductions in weakly bonded species could result in an enhanced carrier mobility.

Figure 4a shows the TCAD simulation results of the control ZnON and Ta-capped ZnON TFTs. Three kinds of states consisting of an exponential acceptor-like tail state (g_{TA}), gaussian acceptor-like deep state (g_{DA}), and gaussian shallow donor-like state (g_{SD}) were considered to fit the I-V characteristics of both devices.

From the TCAD simulation, the extracted key parameters were summarized in Table 3 and each component was depicted in Figure 4b. Because the overall DOS distribution below E_C was dominated by the acceptor-like tail state, the filling of gate field-induced carriers into the localized trap states below E_C occurred

effectively for the Ta-capped ZnON device due to a much smaller g_{TA} distribution. Thus, a higher carrier mobility was expected for the Ta-capped ZnON device, which was consistent with the experimental IV result. It could be clearly seen that the smaller acceptor-like trap density and larger Ne value for the Ta-capped ZnON channel region result in an elevation of the Fermi energy level toward E_C under thermal equilibrium conditions (see Figures 5a, b). A contour of the current density for both devices calculated from the TCAD simulation can be seen in Figures 5c, d. The current density profile of the control ZnON TFTs was uniform along the channel length direction in which the largest current density occurred near the dielectric/channel interface. By contrast, the Ta-capped device exhibited bulk accumulation-like transport in the ZnON channel layer under the Ta-capped region; facile elevation of the quasi-Fermi level as a result of a lower trap state distribution and large Ne value widened the effective channel thickness considerably. Therefore, the total injected current density from the source electrode into the channel region was enhanced, leading to an improved apparent field-effect mobility of the Ta-capped ZnON TFTs.

4 CONCLUSIONS

In summary, the use of TaO_x films as a scavenging and encapsulation layer has been presented; the film could be produced via deposition from a Ta target using DC sputtering followed by a modest annealing process. The volume fraction of nanoscale ZnON crystallites, which were dispersed within an amorphous matrix, was diminished along the depth direction for the control ZnON film. The TaO_x/ZnON stack resulted in uniform crystallization of the overall ZnON films as well as an enhanced stoichiometric Zn_3N_2 portion with less defect centers and a higher free electron density. The transistor fabricated using a TaO_x passivation layer exhibited an excellent mobility of 89.4 cm^2/Vs and a good $I_{ON/OFF}$ ratio of 8.6×10^8, which could be explained by the scavenging effect of non-stoichiometric anion-related defects and encapsulation capability during and/or via TaO_x formation. This improvement was confirmed through TCAD simulation. Bulk accumulation-like transport in the ZnON channel layer under the Ta-capped region greatly contributed to boosting the drain current, which occurred due to facile elevation of the quasi-Fermi level as a result of a lower acceptor-like trap state distribution and large N_e value. The promising effects of Ta capped ZnON TFTs were also confirmed by their superior aging characteristics compared to the control ZnON TFTs. Therefore, the novel encapsulation method using protective TaO_x formation could be a useful route for producing high-performance and reliable ZnON TFTs.

REFERENCES

[1] Ye, Y.; Lim, R.; White, J. M. High Mobility Amorphous Zinc Oxynitride Semiconductor Material for Thin Film Transistors. *J. Appl. Physics*. **2009**, *106*, 074512.

[2] Kim, H.-S.; Jeon, S. H.; Park, J. S.; Kim, T. S.; Son, K. S.; Seon, J.-B.; Seo, S.-J.; Kim, S.-J.; Lee, E.; Chung, J. G.; Lee, H.; Han, S.; Ryu, M.; Lee, S. Y.; Kim, K. Anion Control as a Strategy to Achieve High-mobility and High-stability Oxide Thin-film Transistors. *Sci. Rep*. **2013**, *3*, 1459.

[3] Gao, H.; Zhang, X.; Zhao, Y.; Yan, B. The Correlation of Material Properties and Deposition Condition of ZnON Thin Films. *AIP Adv*. **2017**, *7*, 025111.

[4] Lany, S.; Zunger, A. Anion Vacancies as a Source of Persistent Photoconductivity in II-VI and Chalcopyrite Semiconductors. *Phys. Rev. B* **2005**, *72,* 035215.

[5] Lee, E.; Benayad, A.; Shin, T.; Lee, H.; Ko, D. S.; Kim, T. S.; Son, K. S.; Ryu, M.; Jeon, S.; Park, G. S. Nanocrystalline ZnON; High Mobility and Low Band Gap Semiconductor Material for High Performance Switch Transistor and Image Sensor Application. *Sci. Rep.* **2014**, *4*, 4948.

[6] Ok, K. C.; Jeong, H. J.; Kim, H. S.; Park, J. S. Highly Stable ZnON Thin-Film Transistors With High Field-Effect Mobility Exceeding 50 cm^2/Vs. *IEEE Electron Device Lett.* **2015,** *36*, 38-40.

[7] Jang, J. T.; Park, J.; Ahn, B. D.; Kim, D. M.; Choi, S. J.; Kim, H. S.; Kim, D. H. Study on the Photoresponse of Amorphous In-Ga-Zn-O and Zinc Oxynitride Semiconductor Devices by the Extraction of Sub-Gap-State Distribution and Device Simulation. *ACS Appl. Mater. Interfaces* **2015**, *7*, 15570-15577.

[8] Kuan, C. I.; Lin, H. C.; Li, P. W.; Huang, T. Y. High-Performance Submicrometer ZnON Thin-Film Transistors with Record Field-Effect Mobility. *IEEE Electron Device Lett.* **2016**, *37*, 303-305.

[9] Lee, E.; Kim, T.; Benayad, A.; Kim, H.; Jeon, S.; Park, G. S. Ar Plasma Treated ZnON Transistor for Future Thin Film Electronics. *Appl. Phys. Lett.* **2015**, *107.* 122105.

[10] Shin, Y.; Kim, S. T.; Kim, K.; Kim, M. Y.; Oh, S.; Jeong, J. K. The Mobility Enhancement of Indium Gallium Zinc Oxide Transistors via Low-temperature Crystallization using a Tantalum Catalytic Layer. *Sci. Rep.* **2017**, *7*. 10885.

[11] Kuriyama, K.; Takahashi, Y.; Sunohara, F. Optical band gap of Zn_3N_2 films *Phys. Rev. B*. **1993**, 48, 2781-2782.

[12] Tabet, N.; Faiz, M.; Al-Oteibi, A. XPS Study of Nitrogen implanted ZnO Thin Films Obtained by DC-magnetron Reactive Plasma. *J. Electron Spectrosc. Relat. Phenom.* **2008**, *163*, 15−18.

[13] Cao, X.; Sato, A.; Ninomiya, Y.; Yamada, N.

Oxygen-Doped Zinc Nitride as a High-Mobility Nitride-Based Semiconductor. *J. Phys. Chem. C* **2015**, 119, 5327– 5333.

Table 1. Relative chemical composition of the control and Ta-capped ZnON films obtained via XPS analyses.

	Chemical states	Control ZnON	Ta-Capped ZnON
N 1s	Non-stoichiometric Zn_xN_y	46.8%	38.7%
	Stoichiometric Zn_3N_2	42.7%	52.1%
	N-N bond	10.4%	9.2%
O 1s	Zn-O bond	88.1%	89.5%
	V_O	5.7%	7.8%
	Impurity (OH)	6.2%	2.7%

Table 2 Transfer characteristics of the (a) control ZnON TFT and (b) Ta-capped ZnON TFTs.

Samples	μ_{FE} (cm^2/Vs)	SS (V/decade)	V_{TH} (V)	$I_{ON/OFF}$
Control ZnON TFT	36.2 ± 1.8	0.28 ± 0.04	1.28 ± 0.89	2.9×10^8
Ta-capped ZnON TFT	89.4 ± 9.2	0.33 ± 0.14	-0.45 ± 1.17	8.6×10^8

Table 3 Key parameters of the control ZnON and Ta-capped ZnON TFTs used during simulation.

	Control ZnON TFT	Ta-capped ZnON TFT
N_{TA} [$cm^{-3}\cdot eV^{-1}$]	4.0×10^{19}	1.0×10^{19}
kT_{TA} [eV]	0.025	0.025
N_{DA} [$cm^{-3}\cdot eV^{-1}$]	3.0×10^{17}	1.0×10^{17}
kT_{DA} [eV]	0.3	0.3
N_{SD} [$cm^{-3}\cdot eV^{-1}$]	1.0×10^{17}	4.0×10^{17}
kT_{SD} [eV]	0.1	0.1
E_{SD} [eV]	1.21	1.21
N_e [cm^{-3}]	1.5×10^{17}	2×10^{18}
μ_{band} [$cm^2\ V^{-1}\cdot s^{-1}$]	45	45

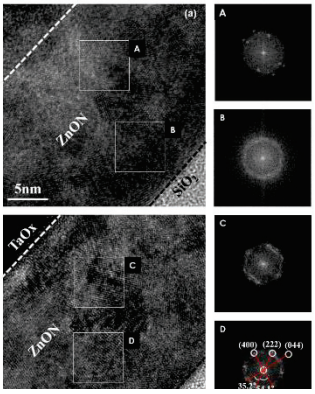

Fig. 1 Cross-sectional TEM images of the (a) control ZnON film and (b) Ta-capped ZnON film. The inset shows a Fast Fourier Transform (FFT) of the selected area, confirming the nanoscale crystallinity of the film.

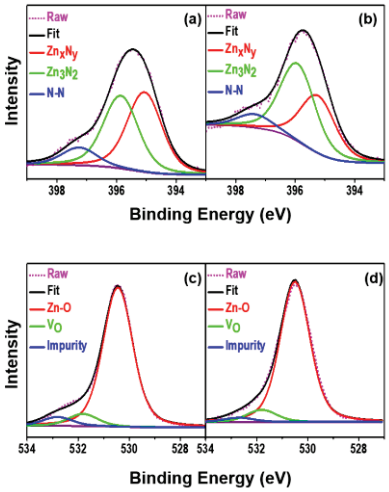

Fig. 2 N 1s XP spectra of the (a) control ZnON film and (b) Ta-capped ZnON film. O 1s XP spectra of the (c) control ZnON film and (d) Ta-capped ZnON film.

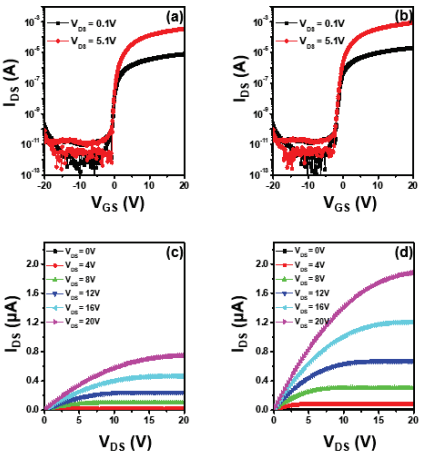

Fig. 3 Transfer characteristics of the (a) control ZnON and (b) Ta-capped ZnON TFTs. Output characteristics of the (c) control ZnON and (d) Ta-capped ZnON TFTs.

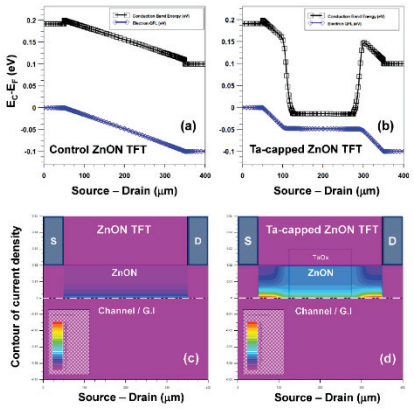

Fig. 5 (a), (b) Simulated energy-band diagrams for the control ZnON and Ta-capped ZnON TFTs. (c), (d) Current density according to the position of the ZnON TFT and Ta-capped ZnON TFT at V_{DS} = 0.1 V and V_{GS} = 4 V.